GLOBAL 4-D INVESTIGATION OF WATER DURING THE MARS YEAR 34 DUSTY SEASON FROM A MULTI-SPACECRAFT ASSIMILATION

J. A. Holmes, S. R. Lewis, M. R. Patel, J. Alday, *School of Physical Sciences, The Open University, Milton Keynes, UK (james.holmes@open.ac.uk)*, **S. Aoki**, *Graduate School of Frontier Sciences, The University of Tokyo, Kashiwa, Japan*, **G. Liuzzi, G. L. Villanueva**, *NASA Goddard Space Flight Center, Greenbelt, MD, USA*, **M. M. J. Crismani**, *California State University, San Bernardino, Department of Physics, CA USA*, **A. A. Fedorova, O. Korablev**, *Space Research Institute of the Russian Academy of Sciences (IKI RAS), Russia*, **K. S. Olsen**, *Department of Physics, University of Oxford, Oxford, UK*, **D. M. Kass**, *Jet Propulsion Laboratory, California Institute of Technology, USA*, **A. C. Vandaele**, *Royal Belgian Institute for Space Aeronomy, Belgium*.

Introduction:

To understand the evolving martian water cycle and variations in transport of water throughout the atmosphere on several timescales (diurnal to seasonal), a global perspective of the combined vertical and horizontal distribution of water is needed. The global 4-D vertical water vapour distribution is investigated through a reanalysis that unifies water, temperature and dust retrievals from several instruments on multiple spacecraft throughout Mars Year (MY) 34 with a global circulation model. The global dust storm and southern summer regional dust storm events pushed water vapour higher in altitude across all latitudes, and supersaturated water vapour is found to penetrate the northern winter polar vortex. This analysis provides new insights into water loss from the atmosphere throughout time and helps to further constrain estimates of the past water inventory on Mars

The past inventory of water on Mars is largely unconstrained as a result of the currently incomplete understanding of how much water has escaped from the atmosphere over time and the processes through which this phenomenon occurs [1,2]. More complete knowledge of how the water inventory has been altered over time requires a better understanding of the past and present atmospheric water cycle and vertical mobility of water vapour. Over the past 50 years orbital and, more recently, surface observations gathered by several missions have helped to build up a more complete description of the seasonal trend and interannual variations in the water cycle through observations of the water vapour column by several different spacecraft [3-9]. One of the outstanding questions regarding the water cycle is a complete understanding of the seasonal evolution of the vertical distribution of water vapour that has a large impact on the transport of water in the atmosphere and surface-regolith interactions [10].

Until recently, the seasonal evolution of the water vapour profile had been observed primarily from spatially sparse SPICAM profiles [7,11] that discovered the presence of supersaturation in the atmosphere of Mars. Supersaturation allows water vapour to propagate through the hygropause, impacting the escape of water from the martian atmosphere. Systematic mapping of the presence of supersaturation, in particular across a complete diurnal cycle, has not yet been conducted but is important to understand how prevalent supersaturation is on Mars. Recent increasingly expansive water vapour profile datasets have been retrieved from instruments on the ExoMars Trace Gas Orbiter (TGO) spacecraft [12,13] illustrating the impact of a global dust storm event on the water vapour vertical structure and further evidence of supersaturation. However, restrictions in space and time mean they cannot provide a truly global perspective.

A global circulation model (GCM) can be utilised for interpretation and understanding of the observed seasonal and latitudinal variations in a global sense. They do however also contain errors of representation associated with computational constraints, meaning it is impossible to completely represent all the physical processes occurring across the globe on local scales (10s of kilometres and below); GCMs can never fully replicate the evolving atmosphere of Mars. Obtaining the best possible analysis of the global evolution of the water cycle requires combining observational data with a Mars GCM. This technique, called data assimilation, is widely used in conjunction with Earth GCMs and three different Mars reanalysis datasets are now publicly available [14,15,16].

In this study we investigate the global distribution of water vapour and the saturation state of the atmosphere throughout L_S = 159-358° in MY 34 utilising a global reanalysis that combines spacecraft observations from several instruments with a Mars GCM.

Spacecraft observations:

This study uses a multi-spacecraft assimilation approach that combines a Mars GCM with retrievals from the ExoMars TGO and Mars Reconnaissance Orbiter (MRO) spacecraft currently in orbit around Mars. Retrieval datasets of water vapour vertical profiles [12,17] and water vapour column [18] are included from the Nadir and Occultation for Mars Discovery (NOMAD) instrument. The Atmospheric Chemistry Suite (ACS) retrieved temperature and water vapour profiles in the near-infrared [13] and mid-infrared [19,20] that are also incorporated into

the reanalysis. Mars Climate Sounder (MCS) [21] retrieved temperature profiles are also incorporated into the assimilation [22-24].

Differences in the orbits of these spacecraft result in a largely complementary expanded dataset when combined due to the minimal overlap in data at the same local time and spatial location, with the coverage of all datasets shown in Figure 1. Data assimilation therefore is a highly efficient method in these circumstances to provide the best possible reproduction of the global atmospheric evolution during this time period.

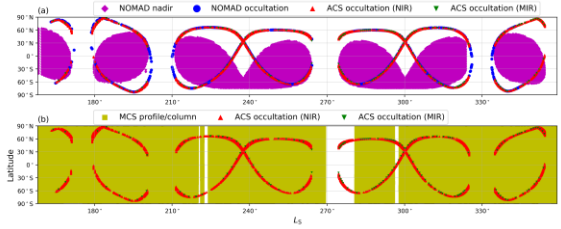

Figure 1 – Coverage of the (a) water vapour and (b) thermal observations included in the global reanalysis.

Modelling and data assimilation:

The reanalysis created through this study incorporates a Mars GCM used by the Open University (OU) modelling group that has been developed in a collaboration between the LMD, the OU, the University of Oxford and the Instituto de Astrofísica de Andalucía. Physical parameterisations [25] and the LMD photochemical module [26,27] both shared with the LMD Mars GCM are coupled to a spectral dynamical core and semi-Lagrangian advection scheme [28]. Specific physical parameterisations linked to the water cycle include the cloud microphysics package [29] that incorporates nucleation on dust particles and supersaturation, an implementation for radiatively active clouds [30], a semi-interactive two-moment scheme to transport dust [31] and a thermal plume model for better representation of turbulence in the planetary boundary layer [32].

The reanalysis produced by this study utilises the Mars GCM truncated at wavenumber 31 (resulting in a 5° longitude-latitude grid in the horizontal for physical variables) with 70 vertical sigma levels that can extend to around 100 km.

To combine the retrieval datasets with the Mars GCM, the Analysis Correction (AC) scheme 3[3] is used (with necessary parameters adapted to martian conditions) that has previously been used to investigate several martian atmosphere scientific topics. The AC scheme is a form of successive corrections in which analysis steps are interleaved with each model dynamical time step. In each analysis step, the analysis increments are spread from the observation locations to the surrounding model grid points with subsequent derivation of multi-variate increment fields for dynamical balance where applicable (e.g. after assimilating temperatures, balanced thermal wind increments are applied).

Validation of the reanalysis dataset:

To validate the water vapour distribution produced by the reanalysis, it was compared against SPICAM data [9] that were not assimilated. An added advantage of data assimilation is that the reanalysis can be compared to retrievals that are not necessarily in the same location as the retrievals combined with the Mars GCM, but nevertheless are still influenced by assimilation of temperature profiles, dust column, and potentially even water vapour profiles in the past.

Figure 2 displays a comparison of SPICAM profiles to the reanalysis and a free running GCM at the closest spatial location and local time. The reanalysis is efficient at reducing the overestimation of water vapour at higher altitudes that is a common problem for GCMs that include supersaturation and is also in very good agreement with the abundance and shape of SPICAM profiles. The validation indicates the reanalysis dataset is the optimal dataset to use for investigating the water cycle, as it captures realistic vertical structures in the atmospheric water profiles.

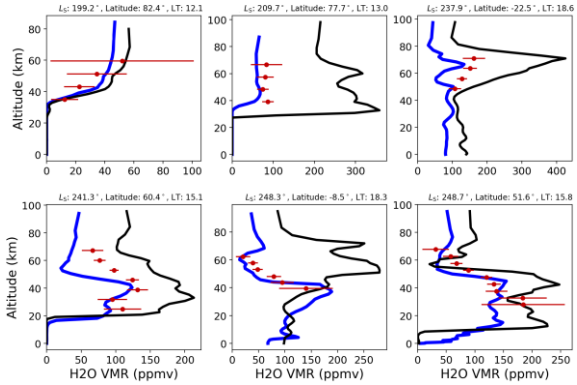

Figure 2 – Comparison of water vapour profiles from SPICAM (red) with independent coincident water vapour profiles in the reanalysis (blue) and a free running GCM (black). Red horizontal bars indicate uncertainty on each altitude point of the retrieval.

Results:

The vertical distribution of water is highly variable and dependent on the season and latitudinal location, as illustrated in Figure 3 which displays the 30° zonally averaged vertical profile of water vapour at a selection of different latitude bands (30° latitudinal means) over time. The global dust storm that occurred from L_S = 180-225° and the intense southern summer regional dust storm from L_S = 320-335° both provided an increased abundance of water vapour to the upper atmosphere at all latitudes including the northern polar region. During the onset of the MY 34 global dust storm, wave activity controls the transport of water poleward of 30°N and 30°S, with wave activity generally acting to transport water vapour polewards in each hemisphere. The hygro-

pause (defined as the highest point at which water is present at 50 ppmv or above) has risen considerably since the start of the simulation and is beyond 50 km during the initiation phase of the global dust storm.

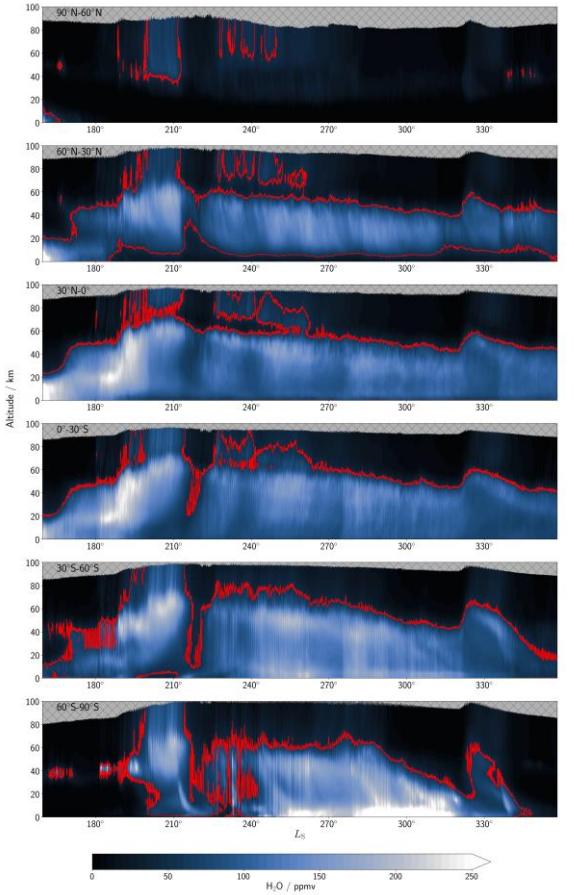

Figure 3 – Zonally-averaged water vapour profiles averaged over 30° latitudinal bands in the water reanalysis. The red line approximates the hygropause location (50 ppmv).

Sublimation of water ice releasing vapour from the southern polar cap in southern summer is evident from L_S = 255-315° in the 60°S-90°S latitude band. While northern polar latitudes (90°N-60°N latitude band) are largely absent of water vapour below 20 km during the dusty season of MY 34, water vapour is found in a middle atmosphere layer reaching the northern pole. The variations in water vapour above 20 km are linked to transport from mid-latitudes via stationary and transient eddies during a global dust storm, perihelion season and the intense MY 34 southern summer regional dust storm. Water vapour at the start of the simulation in the 60°S-90°S latitudinal band is only seen in a band at around 40 km altitude. This water vapour layer is linked to the anticlockwise cell transporting water vapour from lower latitudes into this region.

New evidence is found of water vapour, in a supersaturated state, breaking into the northern winter polar vortex. Figure 4 displays the vertical structure of northern hemisphere water vapour and atmospheric temperature during northern polar winter focused on a 10-sol period around L_S= 250°. The increased water vapour abundance (above 50 ppmv) directly over the north pole above around 40 km is linked to the polar warming and meridional circulation pattern during this time of year in which water vapour is transported northward by transient and stationary eddies rather than the mean meridional circulation. This finding has implications for the surface-atmosphere exchange of water between the northern polar cap and the large-scale atmosphere (via transport of water vapour) and would also have a potential impact on how much water was present in the past atmosphere of Mars if the breaking of supersaturated water into the northern polar vortex is happening repeatedly each Mars year. The results here suggest that the seasonal flux of water vapour into the northern polar cap could be larger than previously thought.

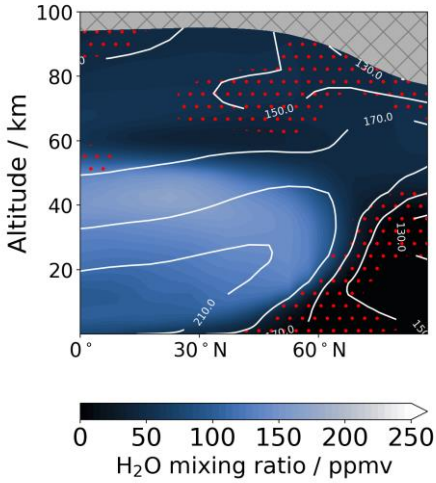

Figure 4 – Zonally-averaged latitude-altitude cross-section of water vapour vertical distribution and atmospheric temperature (white contours) at L_S = 250° in the reanalysis. Red dots indicate the presence of supersaturated water vapour.

References:

[1] Villanueva et al. (2015), *Science Advances*, *7*, 7. [2] Jakosky et al. (2018), *Icarus*, *315*, 146-157. [3] Smith et al. (2004), *Icarus*, *167*, 148-165. [4] Tschimmel et al. (2008), *Icarus*, *195*, 557-575. [5] Smith et al. (2009), *J. Geophys. Res. (Planets)*, *114*, E00D03. [6] Sindoni et al. (2011), *Planet. Space Sci.*, *59*, 149-162. [7] Maltagliati et al. (2011), *Science*, *333*, 1868. [8] Trokhimovskiy et al. (2015), *Icarus*, *251*, 50-64. [9] Fedorova et al. (2021), *J. Geophys. Res. (Planets)*, *126*, e06616. [10] Steele et al. (2017), *Icarus*, *289*, 56-79. [11] Maltagliati et al. (2013), *Icarus*, *223*, 942-962. [12] Aoki et al. (2019), *J. Geophys. Res. (Planets)*, *124*, 3482-3497. [13] Fedorova et al. (2020), *Science*, *367*, 297-300. [14] Montabone et al. (2014), *Geosci. Data J.*, *1*, 129-139. [15] Greybush et al. (2019), *Geosci. Data J.*, *6*, 137-150. [16] Holmes et al. (2020), *Planet. Space.*

Sci., *188*, 104962. [17] Villanueva et al. (2021), *Science Advances*, *7*, eabc8843. [18] Crismani et al. (2021), *J. Geophys. Res. (Planets)*, *126*, e2021JE006878. [19] Alday et al. (2021), *Nature Astronomy*, *5*, 943–950. [20] Olsen et al. (2021), *Astron. Astrophys.*, *647*, A161. [21] McCleese, D. J. et al. (2007) JGR, 112, E05S06. [22] Kleinböhl, A. et al. (2009) JGR, 114, E10006. [23] Kleinböhl, A. et al. (2011) JQSRT, 112, 1568-1580. [24] Kleinböhl, A. et al. (2017) JQSRT, 112, 511-522. [25] Forget et al. (1999), *J. Geophys. Res.*, *104*, 24155-24176. [26] Lefèvre et al. (2004), *J. Geophys. Res.*, *109*, E07004. [27] Lefèvre et al. (2008), *Nature*, *454*, 971-975. [28] Newman et al. (2002), *J. Geophys. Res.*, *107*, 5123. [29] Navarro et al. (2014), *J. Geophys. Res. (Planets)*, *119*, 1479-1495. [30] Madeleine et al. (2012), *Geophys. Res. Lett.*, *39*, L23202. [31] Madeleine et al. (2011), *J. Geophys. Res. (Planets)*, *116*, 11010. [32] Colaïtis et al. (2013), *J. Geophys. Res. (Planets)*, *118*, 1468-1487. [33] Lorenc et al. (1991), *Quart. J. Royal Meteorol. Soc.*, *117*, 59-89.